Guided Microwaves Electromagnetic Drag over the Sensitivity Threshold Experimental Observation

KIRILL ZEYDE, VADIM SHAROV, MIKHAIL RONKIN
Department of radioelectronics and telecommunication
Ural Federal University
Ekaterinburg, Mira street, 32
RUSSIA
k.m.zeyde@urfu.ru

Abstract: - We give a detailed description of our experimental studies of the electromagnetic dragg effect under the laboratory conditions. Our main goal is to show the criteria for an experiment to the successful observation of a small effect versus noise and errors. We use X-band rectangular waveguide, in the cavity of which a dielectric pipe is placed, in which a flow of liquid is achieved. The S_{11} parameters of the circuit are measured using a vector network analyzer. The experimental study is divided into three parts: pilot experiment, preliminary experiment, and target experiment. We describe in detail the stages of experiment designing, as well as the algorithm for experimental data processing. Expectations for the experiment results, we get from the semi-analytical solution of a scattering problem. To describe the effect, we apply an adapted strict solution to the electromagnetic waves propagation in moving media. In conclusion, the internal and external validity of the study is discussed. The distinctiveness of the effect is proved, despite the fact that the flow velocities are relatively low and are about 2 and 3 m/s. The frequency band in which it was possible to observe the effect is quite narrow and approximately equal to 1.25% of the X-band. We propose to use the results of our target experiment as initial data for a pilot experiment of our future studies, and as a consequence, the application of the effect in practice, especially in problems of a radio flow measurement and flow velocity profiles reconstruction.

Key-Words: - Design for experiments, Electromagnetic measurements, Fluid flow measurement, Measurement errors , Microwave propagation, Relativistic effects, Remote monitoring, Transmission line measurements

1 Introduction

This paper presents an experiments series to observe the effect of the special theory of relativity, namely Fresnel drag. Related experiments carried out previously, presented in the works [1] and [2]. We see the following fundamental differences of our experiment: firstly, we conduct an experiment on the microwave, not in the optics; secondly, we are exhausting the effect on guided waves, not in free space. This become possible due to the work carried out earlier: development of a rigorous mathematical formulation of the considered problem [3], [4] and its interpretation model for numerical simulation [5], [6]; and finally, the method of high-sensitive waveguide measurements development and its numerical verification [7], [8]).

The meaning of this work is to prove the observability of relativistic effects on common laboratory equipment, without the use of special tools. The practical significance of such a study was designated in open sources repeatedly [2], [6], [9], [10], [11]. We proceed from the fact that the possible applicability of the effects consists in flow rate measuring. Particular importance consist in the flow profile restoration [9], [10], [11].

Our only target effect is the Fresnel electromagnetic drag [1], [2], [12]. However, it is obvious that in the experiment course a huge number of side effects occur. The restoration of the flow profile is possible only with a successful reconstruction of the dielectric constant of the moving medium, the change in which relatively to the stationary observer is caused only by the Fresnel drag. The analogy with Fizeau's classic experiment is logical [1], [2], [12], [13].

The analytical solution of the electromagnetic waves propagation in a moving medium is presented in [14]. It should be noted that some of the classic Fizeau experiments have already been carried out with certain modern modifications [15] (we hope that ours may be considered to be another one). Despite the fact that study is considered to be classical, it still has certain merits: theoretical value, is to test new approaches to electrodynamics in materials [12], practical in the implementation of new types of flow metering [9], [10] and educational

in explaining a number of fundamental principles of physics [16].

In essence, the goal of this work is to solve the discernibility problem of a small relativistic effect. A very similar problem was solved by the authors for the Rayleigh particle in the waveguide [7]. The target experiment of this work should give a positive answer on the principle observability of the effect and nothing more. We consider the target experiment of this work as a pilot experiment for the following studies. The main motivation of this study is to use the effects to create instruments for the flow velocity profiles reconstruction. The relevance of such a study has been repeatedly noted by the authors [9], [10], [11].

In section 2 we describe the highlights of this study. We indicate the main prerequisites of the experiment and the general provisions. Section 3 is about experiment designing. We describe in detail the hydrodynamic, electrodynamic, measuring systems. We give the experiment installation protocol and try to predict the side effects. In the section 4, we provide a description of our experiments. We dwell on the data processing algorithm. In the section 5, we present summary results.

2 Generalities

The schematic diagram of the experiment is shown in Fig. 1. The scheme can be divided into two systems: hydrodynamic and electrodynamic. The key element of the hydrodynamic system is the device that creates flow – the pump. Connecting pipes and flow regulators are installed as needed, with the minimum possible number of pressure drops and other flow heterogeneities. The electrodynamic system consists of a rectangular waveguide and measuring equipment – a vector net-work analyzer (VNA). The intersection of the hydrodynamic and electrodynamic systems is the waveguide cavity and for us, it is the observation area (OA).

We use a rectangular waveguide $\approx 22.86 \times 10.16$ mm on the X-band. The limiting frequencies are selected for the single-mode propagating regime (the waveguide section length is more than 2λ before and after the OA). Experiments are performed under the ambient conditions. Generally, in this work, we resort only to classical waveguide measurements approaches [7], [17], [18]. Experimental data are obtained in the form of S11 parametes.
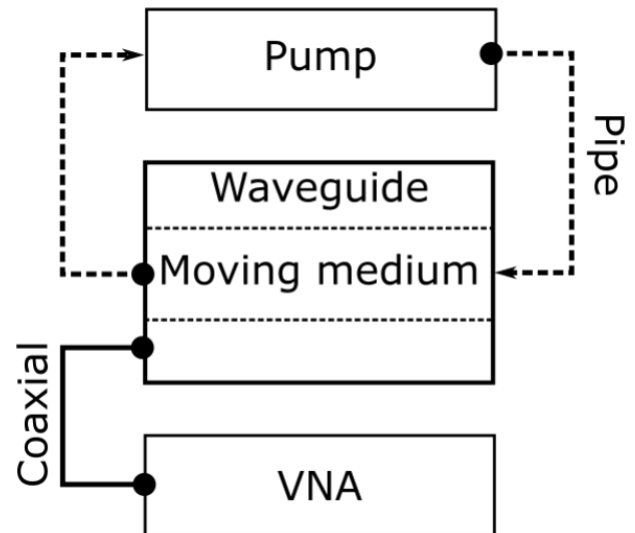
Fig. 1: General structural scheme of the experiment.

We use distilled water as an OA medium. There are three main reasons for this choice. Distilled water is standardized and we have a specification for its dielectric parameters at rest. Thus, we may not carry out additional measurements. Secondly, distilled water is a quite good dielectric with the order of conductivity about 10^{-4}. Low conductivity allows us to apply the results of such studies as [11] and [19]. Finally, distilled water is a calibration medium for high-precision materials parameters measurements on the microwave, as well, [20].

Hereinafter, we use the notation approach from the perturbation theory (such as in [18]). Superscripts 0 and 1 correspond to the values determined at rest and in motion, respectively. One of the classical approaches is the use of a subtract function to establish the target effect. We always use subtraction as follows: $(A^0 - A^1)$, where A – effect magnitude due to perturbation. In our case, the perturbation is the motion of the medium. Indirectly, following the rules of [13], movement changes the dielectric parameters of the medium. This change is a single indicator of the perturbation for us. We introduce the notation: A_{eff} for the magnitude of the electromagnetic drag effect and N_{eff} as its indirect indicator. The meaning of N_{eff} is the magnitude of the change in the refraction index of a moving medium N^1 relative to the resting one N, hence $N_{eff} = N - N^1$.

2.1 Main Positions for Electrodynamics System

We use a strict form of propagation constant in a moving medium [3], [4], [14]. Next, supplement the well-known formula with the guided waves propagation conditions [7]. We indicate the main calculation expressions (note, that γ is propagation constant in moving medium):

$$\gamma = \text{Re}(\gamma_+) + \text{Im}(\gamma_-),$$

$$\gamma_\pm = \frac{-C \pm \sqrt{C^2 + 4k^2}}{2},$$

$$C = V_{flow}\sin\varphi\left(2\omega M - j\mu\omega\varepsilon_0\,\text{Im}[\varepsilon_r]\right),$$

$$M = \frac{N^2 - 1}{c^2},$$

$$k = \omega\sqrt{\frac{\text{Re}(\varepsilon_r)}{c^2} - j\mu\varepsilon_0\,\text{Im}[\varepsilon_r]},$$

$$N = \sqrt{\frac{\text{Re}(\varepsilon_r) + \sqrt{\text{Re}(\varepsilon_r)^2 + \text{Im}(\varepsilon_r)^2}}{2}}.$$

(1)

The last expression needs to be clarified. We do not use the real index of refraction (as in [12], [14] and other related sources) because the propagation medium is dissipative. The imaginary part of the dielectric constant determines not the migration of free charges but the heat loss in the medium, which corresponds to the dielectric conduction model [21] (p. 8). Note that the formula block (1) is a solution of [14] regarding the flow rate V_{flow} and φ for the angle between $\mathbf{V_{flow}}$ and the wave vector $\mathbf{k}$. We specify these values as explained above:

$$\varphi = \arccos\left[\sqrt{1 - \left(\frac{c}{2a_w f}\right)^2}\right],$$

(2)

where a_w = 22.86 mm for our rectangular waveguide.

One of the main tasks is to determine the index of water refraction at rest N. We borrow the necessary data for pure water from [19] and checked it by comparison with the data from [20]. It is well known that water demonstrates a Debye causal characteristic. We use the interpretation with two relaxation frequencies, exactly as in [19]. The decrease of the function is linear and in a given frequency band there is no relaxation process in the medium. Note, that the moving water is a bianisotropic medium [5], [9] with appropriate properties. In this study, we are dealing with weak bianisotropy and this fact must be considered first of all in the numerical simulation [11].

The permittivity of water in motion we express through the propagation constant in the following form:

$$\varepsilon_r^1 = \left(\frac{\gamma c}{\omega}\right)^2.$$

(3)

The value of N^I is found by the last formula in (1) with the value from (3). The target experiment formulated as follows:

$$A_{eff} = F(V_{flow}),$$

(4)

where $F()$ is the response function the explicit form of which we do not define, due to the simulation data (no analytical solution for the considered geometry). Indirect response function $A_{eff} = F(N_{eff})$ in ideal experiment is equivalent to direct. The dependence $N_{eff}(V_{flow})$ established empirically. According to (4), the target value depends on one parameter under control. In the target experiment, there are no random variables. Therefore, we assume that the use of regression analysis is permissible.

Analysis of the basic expressions (1) shows that medium in motion becomes more transparent for electromagnetic waves. The article [3] concluded that $N \geq 1 + \beta^2$. It means that $\left|S_{11}^0(f)\right| > \left|S_{11}^1(f)\right|$, hence $\left|S_{11}^1(f)\right| = \left|S_{11}^0(f)\right| - A_{eff}$. So, we have $A_{eff} = \left|S_{11}^0(f)\right| - \left|S_{11}^1(f)\right|$ is the subtraction function D_i. Equivalent to (4) formulation $D_i = F(N_{eff})$, allows us to get the sensitivity of the experiment by the standard proportion $\dfrac{D_i}{N_{eff}}$. The sensitivity threshold is determined in such a way that the impact response is equal to the total value of experiment uncertainty.

2.2 Main Positions for Hydrodynamics System

In general, the flow rate is decomposed into three values: axial velocity (V_{axial}), radial velocity (V_{radial}) and average volumetric rate [22]. In this paper, under the flow velocity, we consider the last value [23]. Hence,

$$V_{flow} = \frac{Q}{\pi d_{in}},$$

(5)

where Q – volume velocity and d_{in} – pipe inner diameter. It's known, that

$$V_{axial} = \frac{V_{flow}}{\kappa},$$

(6)

where κ - hydraulic coefficient. This coefficient is a function of the Reynolds number (Re) and temperature (T_a). This value is accurately determined only for laminar flow [24]. Next, we fix:

$$Re = \frac{V_{flow} d_{in}}{\nu}, \qquad (7)$$

where ν is a kinematic viscosity. For each of the experimental installations, we must obtain the Reynolds number in order to evaluate the flow: ($2300 \leq Re \leq 4000$) – laminar flow and $Re \geq 10000$ – turbulent flow. In the interval of values, there is a transitional mode [22]. On long-range orders, the turbulent flow has an almost uniform profile and κ → 1 (more accurate dependency is presented in [24]). We expect that in the OA flow will be developed and turbulent. In this regard, the holes cut in the waveguide do not deform the pipe. Flow irregularities are located in more than 10 pipe inner diameters ($\geq 10 d_{in}$) from the OA.

2.3 Main Positions for Simulation

In the work process, we carried out a large number of computational experiments. The initial rules for the simulation were taken from [8]. However, it turned out that accuracy in this approach is insufficient for the task. The main reason for this is a slow convergence of the results of the iterative solver (often exceeding the maximum allowable number of iterations) with the parameter $\Delta S \leq 10^{-5}$ (absolute error for S-parameters). In this regard, we have studied the results of work [11]. Many assumptions and fundamental differences in our work and [11] work impose certain reconciliation restrictions. As shown in [11], the repeatability of simulation results is not guaranteed, since, after a mesh refinement, the problem is solved every time for different numbers of unknowns. In our case, the mesh refinement was carried out at different frequencies in accordance with the sweep rules. Thus, even within the framework of one characteristic $S_{11}(f)$, the uncertainty was unacceptably large. We also considered the possibility of using other numerical approaches. The conclusions outlined in paper [25] were also unsatisfactory for our task.

To circumvent the problem, we make the important indication that the experimenters expectation can only be in the order of magnitude of the effect and not more accurate. To obtain expectations, we use a semi-analytical approach, namely, classical problem solution for electromagnetic wave scattering on an infinite circular cylinder in free space (stated in the variety

of open sources, for example in [26]). Moreover, the problem is solved only once, for a cylinder with a refraction index equal to $1 + N_{eff}$. In the experiment, this is fully consistent with the cavity-perturbation method [18], if we assume that a system without perturbation is a system with a cylinder having free space material parameters ($N = 1$). The resulting value is the electric field scattered from the cylinder – E_{sc}. The field amplitude is searched in close proximity to the cylinder (ρ = raidus + 10^{-12} m) towards infinity. Recalculation formula:

$$\eta_{eff} = 20 \lg\left(\frac{1}{1 - E_{sc}}\right).$$

Under the conditions of our experiment, the use of the infinite cylinder model is justified by the fact that the cylinder does not have end faces in the cavity of the waveguide. The value of the effect magnitude obtained by this method is extremely minimal ($\eta_{eff} > A_{eff}$) and sets the boundary according to the target effect order of smallness. That is why we denoted it η_{eff}. There are a number of ways to reconstruct a diffraction problem from a free-to closed (like a waveguide cavity, or resonator) space. Cylindrical eigenfunctions of waveguide approach is given in [27]. A simple reconstruction for metal and dielectric spheres in the waveguide was performed in papers [7] and [28], respectively. In all cases considered, the proportion $E_{sc} \propto A_{\Delta}$ can be noticed. Here A_{Δ} is an amplitude coefficient, which is absent in expressions for the electromagnetic waves scattering in free space. Moreover, $A_{\Delta} > 1$. The value of this coefficient is related to factors such as multiple reflections (cylinder – wall) and field focusing. Optical approximations are used to determine this value. We rely on experimental data and make the anzats that $\overline{A}_{eff} = A_{\Delta}\eta_{eff}$, $A_{\Delta} = 2.1$.

3 Experiment Setup
3.1 Hydrodynamics System

We use a peristaltic pump GZL-50 as a device that creates a fluid flow. Tests of the pump showed that the flow velocity stabilizes after 2 seconds of operation. From the device specification, it follows that the flow rate error is less than 0.5%. Minimum volume flow equal to 0.5 ml.

Standard dielectric materials for a pipe are used: PTFE (polytetrafluoroethylene) and HDPE (high-density polyethylene). PTFE pipe with din = 5.0 mm is flexible and undergoes deformation under high pressure. The HDPE pipe with din = 5.2 mm does not undergo deformations. We use the following

well known dielectric parameters for pipes: $\varepsilon_r = 2.06$ and $\tan\delta = 0.0002$ for PTFE and $\varepsilon_r = 2.30$ and $\tan\delta = 0.0003$ for HDPE.

The moving medium in the experiment is distilled water (as noted in section 2). We understand that the presence of impurities in it is a guaranteed fact. However, due to the chaotic motion of water molecules, evenly extrapolated to infinity, it gives every reason to believe that the medium at rest is isotropic at the macro level.

3.2 Electrodynamics System

We are trying to ensure the arrival only the fundamental mode to the OA. We use a coaxial waveguide adapter Agilent X281A tested on the discernibility experiments for Rayleigh particles in waveguides [7]. According to the device specification SW R ≤ 1.25 over the entire frequency range. As a matching device, we use a circuit from a forward connected ferrite isolator and an antenna equivalent. Measurements for matching device showed that $|S_{11}| \leq -40$ dB in the whole X-band.

In the port plane, we perform a full one-port calibration according to the algorithm: open, short, match. In this context, particular attention should be paid to the important point: during the experiments, the equipment is calibrated on a waveguide, in the cavity of which is a pipe and water at rest. We do this to minimize external impacts on the laboratory stand. Therefore, measurements with fluid at rest are zero in terms of any effects. This approach, among other things, allows us to adhere the cavity-perturbation concept [18].

We calibrate on an empty waveguide (another section of the waveguide of the same length and without holes for the pipe) only once. Then we compare S_{11} for the waveguide with the pipe and water at rest with the ECAD simulation results. Then we calibrate on a waveguide with a pipe and water at rest and begin the experiment. The data sets are validating by a standardized FSV procedure [29]. In a wide frequency range, success was not achieved. Running a little ahead, we say that the calibration result was validated with the maximum result only in the frequency band in which the target effect was actually measured. So at frequencies between 9.36÷9.41 GHz we get FSV < 0.1.

3.3 Measuring System

As the main measuring device (VNA at fig. (1)) we used Rohde and Schwarz ZVA-50. All measurements are performed at a zero power level. Main description, as well as manipulations we did

with the device, based on information from [30], [31] and [32]. Fundamental measurement provisions can also be found in [21]. With all the experiments, we adhere the same procedure:
• After switching on the device, we wait at least 20 minutes to stabilize the temperature regime.
• Assign start and stop frequencies for analysis – $\Delta f_{analyze}$.
• Set the number of sweep points P_i.
• Select the resolution bandwidth BW.
• Empirical measure a sweep time T_i (if necessary) [31], [32].
• Estimate the noise level of the device (consist of thermal noise -174 dB and internal noise of the generator with assigned BW) [32].
• Carry out a single-port full calibration [30], [32].

Among the presented specifications for the device [31] we are particularly interested in the following information: trace noise of $S_{11} - L_t$, trace temperature stability for $S_{11} - S_t$ and trace repeatability for $S_{11} - R_t$ [32]. We have: $L_t = 0.001$ dB at X-band with BW = 1 kHz, $S_t < 0.05$ dB/K at X-band and $R_t = \pm 0.002$ dB. We do not consider the S_{11} measurement errors, since we assume that the error is duplicated in each of the measurements, as indicated by the parameter R_t. In subtract function, such an error is naturally eliminated.

3.4 Experiment Course

At this stage, the generalized scheme in Fig. 1 should be transformed into the experimental setup scheme. The choice of a particular scheme is based on the experiment design results. We have already done this research [33]. The optimal scheme for the primary drag effect detection is shown in Fig. 2.

The experiment timeline is shown in fig. 3. Timer set in the laboratory – t_{lab}. Within the one measurement with the sequence number n, two phases are distinguished: at rest – $n.0$ and in motion $n.1$. At a random time in $n.0$ phase, a characteristic S_{11}^0 is taken. After that, the pump is turned on. After 2 seconds of flow rate stabilization, the $n.1$ phase begins. In a random period of time S_{11}^1 is taken. The pump turns off and starts measuring with the sequence number $n + 1$.

When conducting a real-time experiment the instrument readings update time is extremely important. In our case, a time sweep T_i occurs. To make S_{11}^1 relevant, it is necessary that an integer number of sweep periods be passed before the $n.1$ phase beginning, hence $N_i T_i$, $N_i \in \mathbb{N}$. More than one
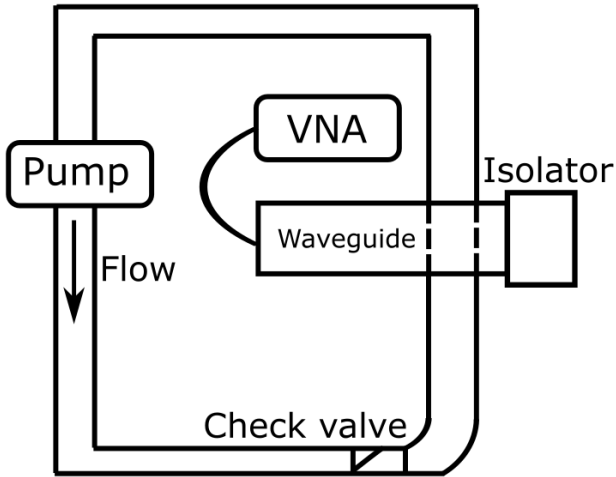
Fig. 2: Scheme of the pilot experiment.
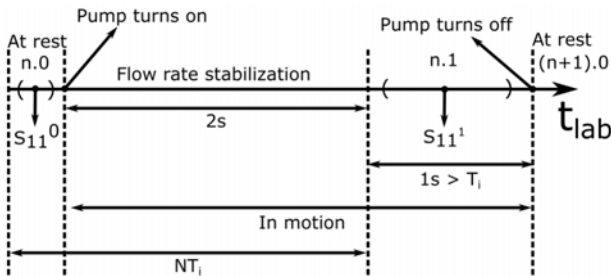
Fig. 3: Experiment timeline.

sweep period should fit into $n.1$ phase also. S_{11}^0 characteristic is taken only after the time T_i after the beginning of the phase $n.0$. We chose the duration of the $n.1$ phase in 1 second based on the heuristic prerequisites for optimal choice. With a relatively short period of time, the probability of erroneous measurement of the flow rate and temperature change in the external environment, liquid during heat exchange with the pump engine and generator is low. This, however, naturally limits us in terms of sweeping time. Value requirement $T_i < 1s$ should be monitored at the calibration stage. Based on the information presented in [30] and [31] $T_i \propto P_i$, $T_i \propto \Delta f_{analyze}$ and $T_i \propto BW^{-1}$. If the latter proportion directly affects the accuracy of measurements and is a critical factor in an experiment, then the other two factors are variable. In fact, an experiment may be successful in detecting an effect at a single frequency (with extreme loss of external validity). In this regard, we can always choose the values of P_i and $\Delta f_{analyze}$ with an unchanged BW to satisfy the T_i requirement.

3.5 Side Effects

Conducting experiments, we will inevitably encounter a number of undesirable effects. We use some provisions from [34] but for closed space. We are trying to predict all possible side effects and divide it into two groups: *a priori* and *a posteriori*. *A priori* effects are those that are present regardless of the laboratory design. In our case, these are internal and thermal noise of the generator, ambient temperature instability, instability of the pump volume flow. It is easy to estimate the error introduced by these effects:

$$\Delta_{error}^{apriori} = L_t + S_t \Delta T_a + \Delta_{mag}^{temp} + \Delta_{mag}^{flow}, \qquad (8)$$

where ΔT_a – the change in ambient temperature during the experiment, Δ_{mag}^{temp} – the change in target effect magnitude associated with ΔT_a and Δ_{mag}^{flow} – the change in target effect magnitude associated with flow caused errors.

Below we describe the apostrioreous side effects we predict:
• The inevitable appearance of impurities in distilled water. The use of standardized distilled water with its regular replacement in the hydraulic system minimizes this effect. The use of a peristaltic pump is also explained by our desire to minimize this effect.
• Elastic deformation of pipes under pressure. Minimized by using rigid pipes.
• Undeveloped flow profile. The elimination of flow irregularities and the increase in straight sections minimizes this effect.
• Vibrations both coaxial cable and OA pipe. We use damping materials to minimize this effect.
• Cavitation. The formation and control of air bubbles in the hydraulic system is described in [35].
• Additional mods. An increase in waveguide lengths contributes to a single mode propagation mode.

4 Experiments
4.1 Processing

For the initial verification of results, we use the simplest point-to-point difference function $D_i(f)$. During data processing, we determine the analysis frequency band by two basic principles: the results of measurements in the statistical population should be repeatable, and $D_i(f)$ in the statistical population should not exceed $\bar{A}_{eff}$ on orders of magnitude. As practice shows, in a narrow frequency band, experimental data can be approximated by linear functions. We use median-median regression: $M_{i,n}(f)$

for each element of the statistical population. The total number of measurements in the experiment – n_{tot}. Statistical population equal to $n_{sp} = n_{tot} - n_{dev}$, where n_{dev} are several first pilot measurements to achieve steady state (high risk of an outlier).

Below we describe the data processing algorithm that we used.

• Determining the frequency range Δf_{mag} of the function $D_i(f)$ according to the $\bar{A}_{eff}$. It makes no sense for us to consider those frequency bands where the subtract function greatly exceeds the magnitude of the effect that we want to observe.

• Check the repeatability of S_{11}^0 measurement in the Δf_{mag} frequency range. We specify the frequency range in which the repeatability is achieved – Δf_{repeat}.

• Next, we carry out a median-median regression of each measurement data to test the hypothesis for Δf_{repeat}.

• For the obtained lines, we determine standard statistics:

$$\bar{M}_i^0(f) = \frac{1}{n_{sp}} \sum_{n=n_{dev}+1}^{n_{sp}} \bar{M}_{i,n}^0(f),$$

$$s^0 = \sqrt{\frac{\sum \left[M_{i,n}^0(f) - \bar{M}_{i,n}^0(f) \right]^2}{n_{sp}-1}}. \quad (9)$$

• Perform a similar operation for S_{11}^1 at Δf_{repeat}. We get the values: $\bar{M}_i^1(f)$ and s^1.

• Compare $\bar{M}_i^0(f)$ and $\bar{M}_i^1(f)$. Define the reliability interval, as

$$\Delta_{rel} = \min\left[\bar{M}_i^0(f) \pm s^0, \bar{M}_i^1(f) \pm s^1 \right]. \quad (10)$$

This interval determines the margin for changing the V_{flow} during the controlled experiment.

• Determine the experimental value of $A_{eff} = \bar{M}_i^0(f) - \bar{M}_i^1(f)$.

4.2 Pilot Experiment

For the pilot experiment, we chose the following parameters: $P_i = 2000$, $\Delta f_{analyze} = 8\text{-}12$ GHz, BW = 10 kHz. Q = 56.6 ml/s, hence $V_{flow} = 2.883$ m/s. $T = 25.5$ºC and $Re = 1.69366 \times 10^4$ for $\nu = 0.851 \times 10^{-6}$ m^2/s. We are dealing with turbulent flow. Statistical data: $n_{tot} = 5$, $n_{dev} = 2$, $n_{sp} = 3$.

The pilot experiment setup is (see Fig. 2): pipe in the observation area – PTFE, all measurements were carried out with a matching device at the second port, a check valve was connected, so the hydraulic

system would not be emptied during the $n.0$ phase. We did not use any thermal insulation or vibrations damping materials. We intend to use coaxial cables that are highly sensitive to phase distortion.

As expected in the pilot experiment, we encountered a whole range of side effects. Its total magnitude was so large that we did not see the point in processing the data to restore the target parameters. Hence, we could not select a Δf_{mag} band. The spread of $D_i(f)$ values in $\Delta f_{analyze}$ was [0.1÷12.5] dB, the minimum value is two orders of magnitude higher than expected.

The first thing we encountered was the jumps in the reflection level after the calibration. Without any external influence at the S_{11}^0 level for a matched load equal to -40 dB, the deviation of the parameter was ±2 dB (we took measurements on a matched line). For a highly sensitive experiment, this is unacceptable. The next side effect was the deformation of the pipe in the cavity of the waveguide under pressure. Flexible PTFE pipe is subjected to a uniform increase in diameter along the entire length of the hydraulic system where it is used. This effect is very similar to the elastic deformation effect of an object under the action of the inertial forces [36]. In some cases, this effect may be beneficial. And the third effect with overwhelming magnitude was an undeveloped flow profile in the waveguide cavity. We used the very standard check valve before directly entering the pipe into the waveguide. We did not take into account this flow heterogeneity, but it turned out that the flow profile after the check valve should be restored by the straight section of the hydraulic system. In this case, the κ coefficient takes the invalid values for us.

4.3 Preliminary Experiment

In the preliminary experiment, we managed to eliminate the main side effects of the pilot experiment. We clarified the frequency band $\Delta f_{analyze} = 9\text{-}10$ GHz and now with $P_i = 6000$, parameter BW remained the same. The laboratory setup foto is shown in Fig. 4. Pipe in the observation area – HDPE. Q =58.3 ml/s, hence $V_{flow} = 2.745$ m/s. $T = 25.5$ºC with $\Delta T_a < 0.1$ºC and $Re = 1.67744 \times 10^4$. Statistical data: $n_{tot} = 10$, $n_{dev} = 3$, $n_{sp} = 7$.

Compared to the first experiment, we abandoned the use of a PTFE pipe subjected to elastic deformation. Instead of a matching device, we carried out measurements on a short line. Thus, the effect is observed on standing waves, as in waveguide resonators [18]. In this case, the position
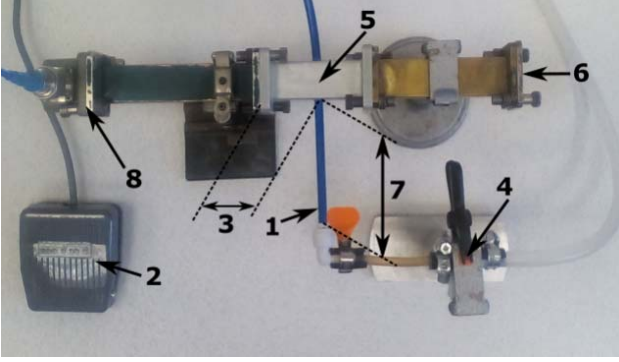
Fig. 4: 1 – pipe, 2 – pump control, 3 – waveguide with length equal to λ at f = 10 GHz, 4 – check valve, 5 – observation area, 6 – short measure, 7 – flow developing path, 8 – coaxial waveguide adapter.

of the pipe in the waveguide cavity relative to its length already matters. We see this clearly during experimental data processing. The last key change in the laboratory stand was the flow developing path. Due to the fact that we used a joint of pipes of 90º, the length of the path is more than $12d_{in}$.

These manipulations led to a significant result. Step-by-step data processing (according to the algorithm proposed in subsection 4.1) of the second experiment is shown in Fig. 5. However, additional side effects were identified during the study. Firstly, vibrations of coaxial cable. Secondly, uneven flow at the pump inlet. We tried to exclude these effects in the target experiment.

4.4 Target Experiment
We obtained the following parameters for our final experiment: $\Delta f_{analyze} = \Delta f_{preliminary\_mag} = \Delta f_{mag} = \Delta f_{repeat}$ = 9.36 ÷ 9.41 GHz with P_i = 1000 and BW = 1 kHz. We have $T_i \approx 0.9$ s, T_a = 26.2ºC, $\Delta T_a \rightarrow 0$ ºC, Q = 70 ml/s, V_{flow} = 3.296 m/s and Re = 2.01407×10⁴. We also improved the installation a bit to control and minimize side effects. First, we use phase-independent coaxial cable that is not sensitive to small vibrations. On the other hand, we eliminate vibrations by damping the pump and supply pipes. Eliminating the check valve from the scheme (4 in Fig. 4) we have increased fluid flow and achieved a more uniform flow profile. In order to maintain a stable pressure in the hydraulic system during $n.0$ phases, we use a buffer tank through which fluid flows to the pump. We have increased the flow development path (7 in Fig. 4) and now it is more then $15d_{in}$. To minimize temperature deviations, we used thermal insulation material on the pipes. Statistical data: n_{tot} = 13, n_{dev} = 3, n_{sp} = 10.

In general, we were satisfied by the results. The results of data processing for the target experiment are shown in Fig. 6a. The effect could be observed visually on the VNA display (Fig. 6b).

5 Results and Discussion
The resulting data for preliminary and target experiments are shown in Tab. 1.

TABLE 1: EXPERIMENTS RESULTS.

Value	Preliminary	Target
Experimental A_{eff}, dB	3.9541 ×10⁻⁴	1.2177 ×10⁻³
η_{eff}, dB	5 ×10⁻⁵	6 ×10⁻⁵
S_{eff}, %	49.60 ÷ 49.75	22.63 ÷ 22.75
$\overline{A}_{eff}$, dB	1.05 ×10⁻⁴	1.26 ×10⁻⁴
Δ_{rel}, dB	1.2000 ×10⁻⁴	8.2850 ×10⁻⁴
$\Delta_{error}^{apriori}$, dB	> 0.010	≈ 0.001
N_{eff}	4.2212579×10⁻⁷÷ 4.2098774 ×10⁻⁷	5.0960794×10⁻⁷÷ 5.0619621 ×10⁻⁷

The mean-square relative error in measuring A_{eff} value is calculated as follows:

$$S_{eff} = \frac{\sqrt{\left(s^0\right)^2 + \left(s^1\right)^2}}{A_{eff}}$$. To determine the unknown

terms in (8), use the following expressions:

$$\Delta_{mag}^{temp} = \frac{N_{temp}\overline{A}_{eff}}{N_{eff}},$$
$$\Delta_{mag}^{flow} = \frac{N_{flow}\overline{A}_{eff}}{N_{eff}}, \quad (11)$$

where N_{temp} is the change in refraction of the medium caused by the change of T_a. This value is easy to obtain from [19]. For T_a = 25.5 ºC, ΔT_a = 0.01ºC and frequency band 9.39÷9.41 GHz, N_{temp} = 0.0000848 and Δ_{mag}^{temp} = 0.021 dB. It is quite obvious that the elimination of any heat exchange of a moving medium is the most important task in setting up an exact experiment. The relatively short time of the experiment is explained by this fact. An imminent change in ambient temperature, however, does not immediately affect on the water temperature.
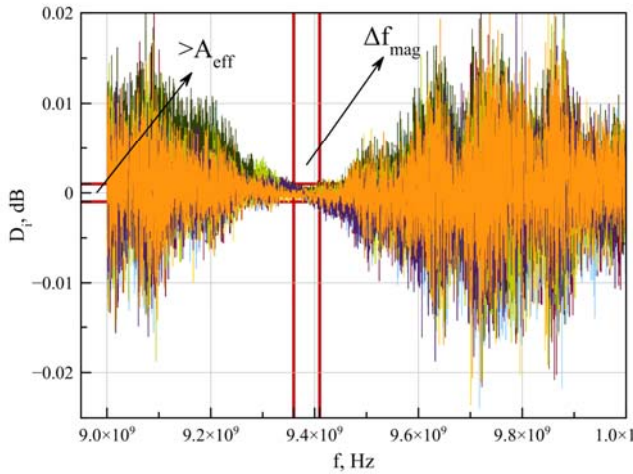
(a) Allocation of the expected effect magnitude frequency band: $A_{eff} = \pm 0.001$ dB, $\Delta f_{mag} = (9.36 \div 9.41)$ GHz.
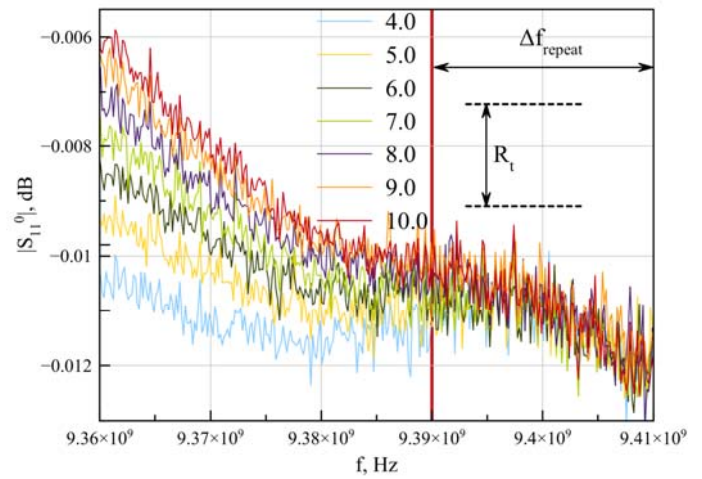
(b) Allocation of the measurements at rest repeatability frequency band: $\Delta f_{repeat} = (9.39 \div 9.41)$ GHz.
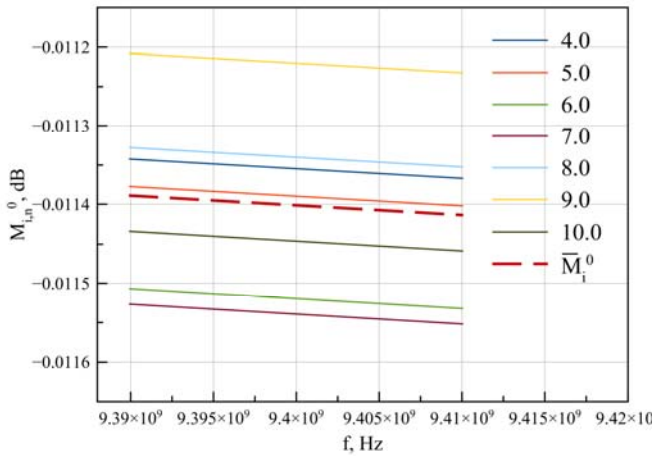
(c) Median-median linear regression of measurements at rest and its medium level.
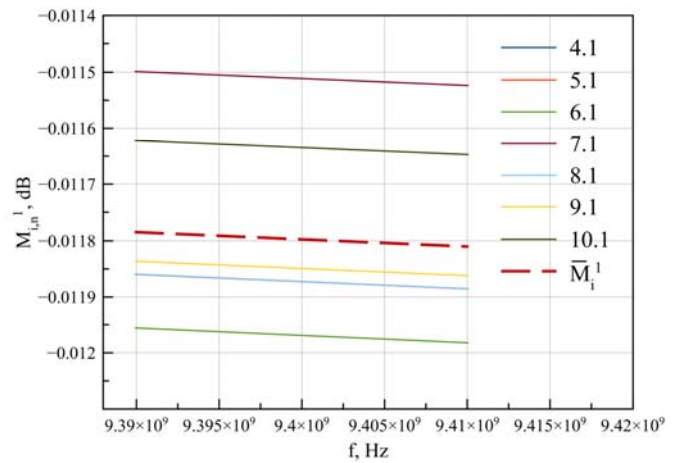
(d) Median-median linear regression of measurements in motion and its medium level.
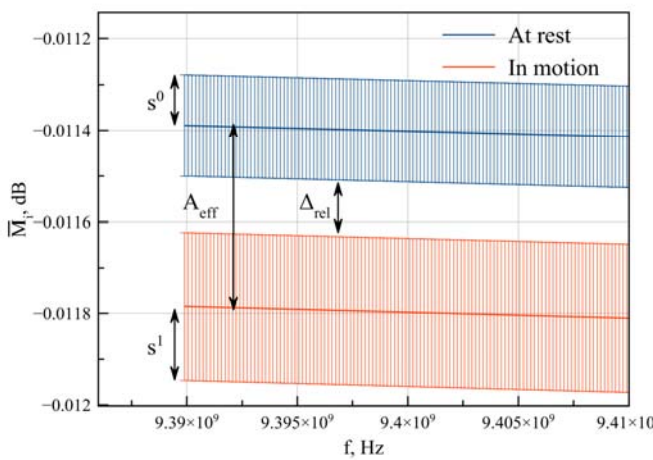
(e) Comparison of median values with error drops: $A_{eff} = 3.9541 \times 10^{-4}$ dB, $s^0 = 1.1086 \times 10^{-4}$ dB, $s^1 = 1.6176 \times 10^{-4}$ dB, $\Delta_{rel} = 1.2000 \times 10^{-4}$ dB.
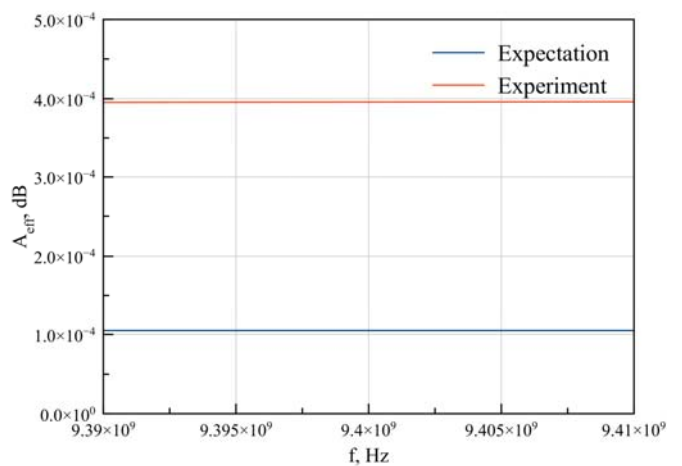
(f) Comparison experimental and simulation results for A_{eff}.

Fig. 5: Preliminary experiment data processing.
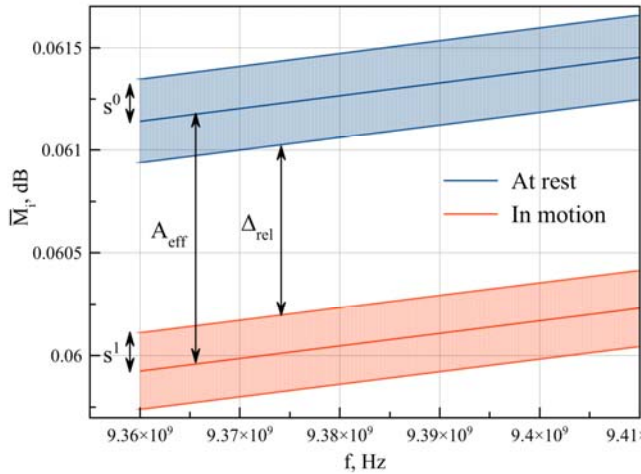
(a) Comparison of median values with error drops: A_{eff} = 1.2177 ×10^{-3} dB, s^0 = 2.0444 ×10^{-4} dB, s^1 = 1.8480 ×10^{-4} dB, Δ_{rel} = 8.2850 × 10^{-4} dB.
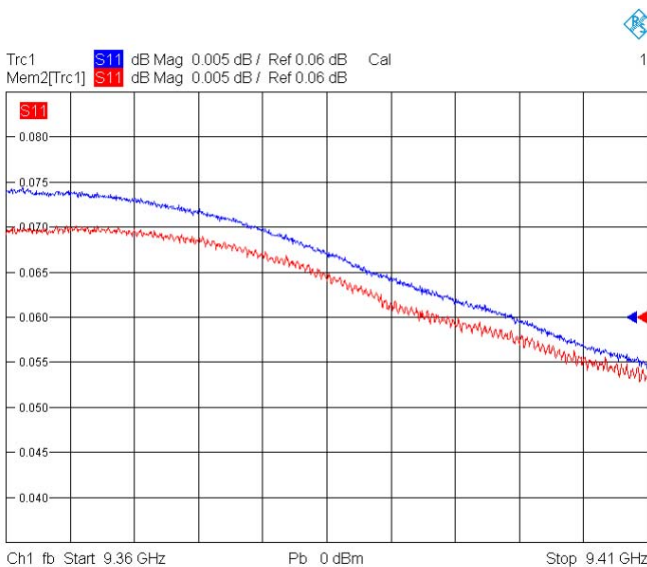
(b) VNA reading on one of the statistical population measurement: blue line – water at rest and red line water in motion.

Fig. 6: The main results of the target experiment.

Subsection 3.1 indicates that the flow output error from the pump is 0.5%. So, for the target experiment, the absolute error is 0.016 m/s . It means that N_{flow} = 2.4572628×10^{-9} and $\Delta_{mag}^{flow} = 6.067 \times 10^{-7}$ dB. We can conclude that this error is reasonably neglected.

Now, we explain the results presented in tab. 1. According to the results of the preliminary experiment, we conclude that the magnitude of the effect corresponds to our expectations. Regression data processing revealed significant errors related primarily to the *a priory* parameters of the

experiment. We see that in such conditions the interval of possible variation of the target value is negligible (Δ_{rel}), and may even be blurred by another statistical population, which was clearly insufficient in our case.

In the target experiment, we increased the flow rate, avoid a number of side effects and *a priori* errors. The magnitude of the effect increased substantially. The standard deviation in the statistical population was halved. We managed to slightly expand the frequency band and it was about 1.25 % of whole X-band. Regressive data processing has made its own adjustments to the dynamics of $S_{11}(f)$ functions, however, this is not a significant moment for us. The key point is the strong mismatch of the expected magnitude. We find two possible explanations for this. The first is an incorrectly made ansatz, relatively A_Δ. And second, the appearance of the side effect due to the increase in the flow velocity, which we did not take into account.

However, the main result of this work is the the fact that we observed a stable response of the measuring equipment to changes in the target value. In this context, expression (4) can be considered confirmed.

6 Conclusion

The observability of the relativistic effect over the sensitivity threshold of the measuring equipment may be a good prerequisite for the development o specific devices for the restoration of the flow profile. We understand that the improvement of both the theoretical part and its practical implementation is an important task in this work. We distinguish three main development directions. The first is to obtain the expected effect value with maximum accuracy. Of course, we should not be limited only by the order of the effect, both from the side of the analysis and measurements. Conducting a continuous experiment with good temperature stability to obtain a sufficiently large statistical population, the next important task. The main problem here is the temperature stability of the VNA. And the last task is to increase the external valdiness of the experiment. Two previous points, partly contribute to this. Nevertheless, it seems to us that a good verification would be the results of an experiment in which the medium moved directly in the cavity of the waveguide. A rectangular waveguide is ideally suited for this purpose, due to the fact that the most uniform flow profile is established in rectangular conduits.

References:

[1] Y. Z. Zhang, Special relativity and its experimental foundation, *Advanced Series on Theoretical Physical Science*, World Scientific, vol. 4, 1997.

[2] J. Van Bladel, *Relativity and engineering*, Springer series in electrophysics, Springer-Verlag, vol. 15, 1984.

[3] K. M. Zeyde, The complete form of the propagation constant in a noninertial reference frame for numerical analysis, *Zhurnal Radioelektroniki – Journal of Radio Electronics*, no. 4, 2019.

[4] K. M. Zeyde, The coordinate expression of the propagation constant for a moving dielectric medium, in *Proc. USBEREIT*, Ekaterinburg, Russia, 2018, pp. 295–298.

[5] K. M. Zeyde, Augmented interpretation model of a moving media for the electrodynamic effects simulation, in *Proc. NEMO*, Reykjavik, Iceland, 2018.

[6] K. M. Zeyde, Fast segmentation of a rotating axisymmetric scatterer medium of an arbitrary form for the first order fields numerical analysis, *Ural radio engineering journal*, vol. 2, no. 2, 2018, pp. 26–39.

[7] K. M. Zeyde, Discernibility of metallic sphere in rectangular waveguide, in *Proc. ACES*, Florence, Italy, 2017.

[8] K. M. Zeyde, Verified simulation of waveguide inhomogeneities in Keysight EMPro 2017 software, *Ural radio engineering journal*, vol. 2, no. 4, 2018, pp. 67–76.

[9] M. Pastorino, M. Raffetto and A. Randazzo, Electromagnetic inverse scattering of axially moving cylindrical targets, *IEEE Trans. on GSRS*, vol. 53, no. 3, 2015, pp. 1452–1462.

[10] M. Brignone, G.L. Gragnani, M. Pastorino, M. Raffetto and A. Randazzo, Noise limitation on the recovery of average values of velocity profiles in pipelines by simple imaging systems, *IEEE GSRS letters*, vol. 13, no. 9, 2016, pp. 1340–1344.

[11] P. K. Ramakrishnan and M. Raffetto, Accuracy of finite element approximations for two-dimensional time-harmonic electromagnetic boundary value problems involving non-conducting moving objects with stationary boundaries, *ACES Journal*, vol. 33, no. 6, 2018, pp. 585–596.

[12] R. Starke and G. A. H. Schober, Microscopic theory of refractive index, *International Journal for Light and Electron Optics*, vol. 140, 2017, pp. 62–85.

[13] P. Beckmann, Equivalent electromagnetic constants of moving media, *Proceedings of the IEEE*, vol. 58, no. 5, 1970, pp. 800–801.

[14] J. R. Collier and C. T. Tai, Propagation of plane waves in lossy moving media, *IEEE Trans. on antennas and propagat.*, vol. 12, no. 3, 1964, pp. 375–376.

[15] O. Morizot, A. Selle, S. Ferri, D. Guyomarch, JM. Laugier and M. Knoop, A modern Fizeau experiment for education and outreach purposes, *European Journal of Physics*, 2011.

[16] J. R. Melcher, Electric fields and moving media, *IEEE Transactions on education*, vol. E-17, no.2, 1974, pp. 100–110.

[17] K. Ogusu, Measurements of dispersion characteristics and field distributions in rectangular-dielectric waveguide and its modifications, *IEEE Trans. on MTT*, vol. MTT-26, no. 3, 1978, pp. 169–171.

[18] P. Banerjee, G. Ghosh and S. K. Biswas, Measurement of dielectric constant of medium loss cylindrical-shaped samples using cavity perturbation method, in *Proc. AMTA*, Jaipur, India, 2008, pp. 124–125.

[19] T. Meissner and F. J. Wentz, The complex dielectric constant of pure and sea water from microwave satellite observations, *IEEE Trans. GSRS*, vol. 42, no. 9, 2004, pp. 1836–1849.

[20] S. Asif, B. Braaten and A. Iftikhar, Effectiveness of a dielectric probe calibration using deionized, distilled and tap water, in *Proc. APIS &USNC/URSI National Radio Science Meeting*, San Diego, CA, USA, 2017, pp. 893–894.

[21] L. F. Chen, C. K. Ong, C. P. Neo, V. V. Varadan and V. K. Varadan, *Microwave electronics measurement and materials characterization*, John Wiley & Sons, 2004.

[22] R. C. Baker, *Flow measurement handbook*, Cambridge University Press, USA, 2000.

[23] M. V. Ronkin and A. A. Kalmykov, Analysis of processing features of ultrasonic flowmeters with FMCW signals, *Ural radio engineering journal*, vol. 2, no. 4, 2018, pp. 52–66. – (in Russian).

[24] Liu Yong-hui, Du Guang-sheng, Tao li-li and Shen Fang, The calculation of the profile linear average velocity in the transition region for ultrasonic heat meter based on the method of LES, *Journal of hydrodynamics*, vol. 23, no. 1, 2011, pp. 89–94.

[25] K.F. Warnick and W. C. Chew, Accuracy of the method of moments for scattering by a cylinder, *IEEE Trans. on MTT*, vol. 48, no. 10, 2000, pp. 1652–1660.

[26] A-K. Hamid and M. AlSunaidi, Inverse scattering by dielectric circular cylindrical scatterers using a neural network approach, in *Digest IEEE APSIS*, Quebec, Canada, 1997, pp. 2278–2281.

[27] V. Kalesinskas, A. Konstantinov and V. Shugurov, Inverse scattering by dielectric circular cylindrical scatterers using a neural network approach, in *Proc. MIKON-98*, Krakow, Poland, 1998.

[28] K. M. Zeyde and V. V. Sharov, Discernibility and MDR for the complex dielectric sphere in rectangular waveguide, in *Proc. APEDE*, Saratov, Russia, 2018, pp. 294–299.

[29] IEEE Standard for Validation of Computational Electromagnetics Computer Modeling and Simulations, IEEE Standard 1597.1, 2008.

[30] R&S ZVA / R&S ZVB / R&S ZVT Vector network analyzers operating manual, Version 31, 2018.

[31] R&S ZVA Vector network analyzers specifications, Version 11, 2014.

[32] M. Hiebel, *Fundamentals of vector network analysis*, 2nd ed., Rohde and Schwarz, Germany, 2018.

[33] K.M. Zeyde and V.V. Sharov, Fluid Flow Sensors Design based on Electromagnetic Drag Effect, in *Proc. ICCAIRO*, Athens, Greece, 2019.

[34] W. Wiesbeck and S. Riegger, A complete error model for free space polarimetric measurements, *IEEE Trans. on antennas and propagat.*, vol. 39, no. 8, 1991, pp. 1105–1111.

[35] Han Biao, Tang Rongming, Wang Xuefang and Xu Hongqing, Bubble content in air/hydro system – part 1: measurement of bubble content, *Tsinghua Science and Technology*, vol. 5, no. 1, 2000, pp. 68–71.

[36] A .R. Ali and T. Ioppolo, Effect of angular velocity on sensors based on morphology dependent resonances, *Sensors*, vol. 14, 2014, pp. 7041–7048.